

Growth behavior of flower-shaped nano-CdS clusters on biomorphic porous carbon (BPC) substrates using a hydrothermal method

Peng-zhao Gao^{a,*}, Zhou-li Lu^a, Hua-nan Lv^a, Wei Liu^{b,*}, Bing Yan^a and Xiao-liang Zhang^a

^aCollege of Materials Science and Engineering, Hunan University, Changsha 410082, China

^bState Key Laboratory of New Ceramics and Fine Processing, School of Materials Science and Engineering, Tsinghua University, Beijing 100084, P. R. China

Flower-shaped nano-CdS clusters grown on biomorphic porous carbon (BPC) substrates have been successfully prepared using a hydrothermal method. Influence of growth time, types of substrate and carbonized temperature on the growth behavior of flower-shaped nano-CdS clusters were studied using XPS, XRD, TGA, and SEM. The results indicated that wurtzite nano-CdS clusters were successfully integrated into the inner wall of BPC with various morphologies: couch grass-shaped clusters can grow on the inner wall of BPC derived from pine, sunflower-shaped clusters can grow on that derived from bamboo and chrysanthemum-shaped clusters can grow on that derived basswood. The crystal size of nano-CdS clusters grown for 24 h on BPC derived from pine was approximately 7 nm. The size and number of nano-clusters grown on BPC substrate were mainly affected by the growth time and the substrate carbonized temperature, respectively. Finally, the growth mechanism of nano-CdS clusters on BPC substrates was also discussed.

Key words: Biomaterials, Semiconductors, Crystal growth, Electron microscopy.

Introduction

CdS is one of the II-VI compounds with unique properties [1]. CdS has promising applications in, for instance, light emitting diodes [2], solar cells [3], optoelectronics [4], and catalysts [5,6]. The properties of CdS materials are greatly affected by the preparation method, particle size, and particle morphology. Presently, nanowires [7], nanorods [8], nanoparticles [9], flower-shaped particles [10], and hexagonal and triangular plates [11] have been prepared using various methods, such as solvothermal synthesis [12], hydrothermal synthesis [13], microwave irradiation [14], chemical deposition [15], and templates [16]. Additionally, these materials usually grow on various substrates, such as glass [17], Si [18], TiO₂ [19], carbon fiber [20], and carbon nanotubes [21].

Compared to other substrates, biomorphic porous carbon (BPC) possesses the following advantages: it has high specific area and abundant organic functional groups, which are propitious to improve both the sensitivity of the sensor and the activity of the catalyzer when BPC behaves as a sensor and catalyst support [22]. The orderly, one-direction through-hole structure is conducive to the transmission of fluid through it; the varied pore diameter distribution provides different transmission channels for different particle sizes [23].

However, few studies in the literature have reported the growth behavior of nano-materials on BPC substrates.

The hydrothermal method is widely used to prepare several types of nano-materials, and it is low-cost, environmentally friendly and able to be performed with simple equipment. The materials obtained using this method possess high purity, crystal integrity, and monodisperse size that is easily controlled [13].

This study investigated the growth behavior of nano-CdS clusters on BPC substrates using a hydrothermal method. The influence of the growth time, type of BPC substrate, and carbonized temperature on the morphology of nano-CdS clusters were studied using several techniques, such as XPS, XRD, TGA, and SEM. Finally, the growth mechanism of CdS clusters on BPC substrates was discussed.

Experiments

Raw materials

The biomorphic porous carbon derived from wood retained its biomass characteristics and was prepared according to reference [24]. The carbonized temperatures used were 450 °C, 600 °C, 750 °C and 900 °C, respectively. The BPC substrate was cut into small blocks of 3 mm × 3 mm × 3 mm. Cadmium chloride hemipentahydrate (CdCl₂·2.5H₂O), sodium sulfide hydrate (Na₂S·9H₂O), polyvinylpyrrolidone (PVP), anhydrous ethylenediamine (H₂NCH₂CH₂NH₂, En) and ethanol (CH₃CH₂OH) were used in this experiment. All chemicals were AR grade. Deionized water was used in this experiment.

*Corresponding author:
Tel : +86-731-88822269
Fax: +86-731-88823554
E-mail: gaopengzhao7602@hnu.edu.cn, liuwei2013@tsinghua.org.cn

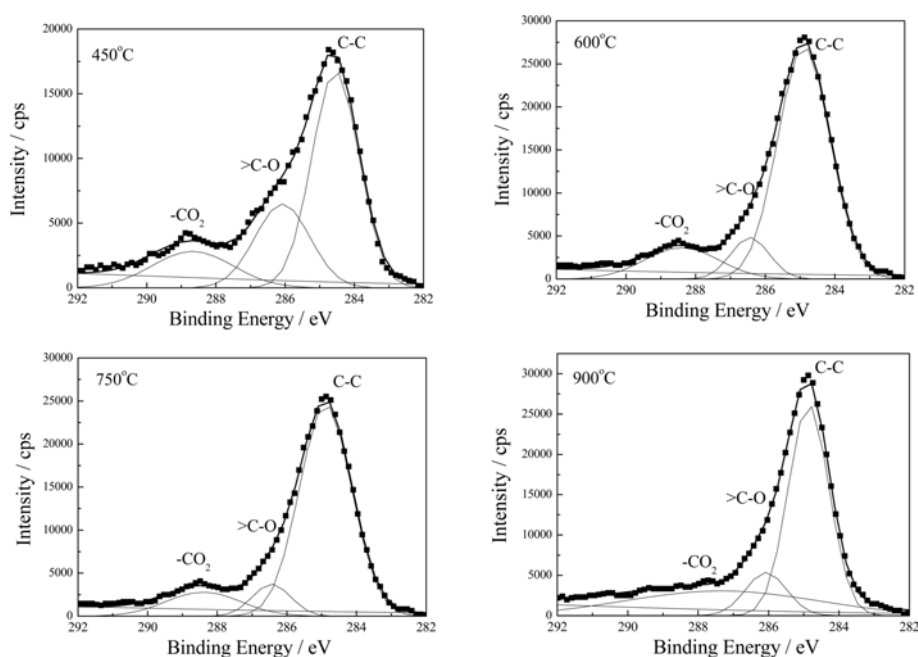


Fig. 1. C_{1s} XPS spectra of pine wood carbonized at different temperatures.

Preparation of nano-CdS clusters on BPC substrate

First, 0.228 g $CdCl_2 \cdot 2.5H_2O$, 0.25 g $Na_2S \cdot 9H_2O$, 0.1 g PVP and blocks of BPC substrate were added to a 25 ml Teflon-lined stainless steel autoclave. Approximately 20 ml of a 25% En aqueous solution (V/V) was added to the reactor capacity. The hydrothermal process was carried out at 180 °C for 12, 24 and 48 h, respectively. The precipitate in the autoclave was collected and then washed 3 times each with ethanol and deionized water. The washing process was performed in a high energy ultrasonic machine after which the precipitate was dried in air at 80 °C for 6 h.

Characterization

The content of the organic groups in BPC obtained at different carbonized temperatures was determined by the fine structure of the C_{1s} binding energy using XPS. The XPS measurements were carried out with a Fisons Escalab 200R Ultra spectrometer, which was equipped with a monochromatic $Mg K_{\alpha}$ X-ray source operating at 150 W and with a delay-line detector. The background pressure was 2×10^{-9} mPa.

The morphology of the nano-CdS/BPC materials was characterized by scanning electron microscopy (SEM, JSM-6700F, Jeol); the microscope was equipped with an energy dispersive spectrometer (EDS, Oxford).

The phase of the nano-CdS/BPC materials was characterized by X-ray diffraction (XRD, D5000, Siemens), using nickel filtered Cu K radiation operating at 30 kV and 30 mA, with a scanning speed of 2°min^{-1} . The crystal size of the nano-CdS was calculated by the Scherer equation (Eq-1):

$$D = \frac{K\lambda}{B \cos \theta} \quad (1)$$

where λ is the wavelength, B is the width at half peak, and K equals 0.89.

The thermal stability of the nano-CdS clusters was characterized using thermogravimetric analysis (TGA) and differential scanning calorimetry (DSC) in an Ar atmosphere with a flow rate of $50 \text{ ml} \cdot \text{min}^{-1}$ and a heating rate of $10^\circ \text{C} \cdot \text{min}^{-1}$ from room temperature to 900 °C. TGA and DSC were performed on a TGA-DSC thermal analyzer (model Netzsch Thermische Analyzer STA 409C) with alumina powder as the reference sample.

Results

Influence of carbonized temperature on the content of organic functional groups in BPC

The C_{1s} XPS spectra of BPC derived from pine carbonized at different temperatures are shown in Fig. 1. The binding energy of C_{1s} possesses different values when different forms of carbon atoms bond with oxygen atoms. The spectra can be according to the corresponding form of carbon atom, and can also be interpreted by the relative content of different organic groups according to a previous study [25], where, $-CO_2$ stands for the oxo-organic functional group $O-C=O$, $C-O$ for both $C-O$ and $C-O-C$, and $C-C$ for the common $C-C$ bond.

In Fig. 1, there are abundant oxo-organic groups in the BPC substrate carbonized at 450 °C with high peak areas of $-CO_2$ and $>CO$. As the carbonized temperature increases, the peak areas of $-CO_2$ and CO decrease, whereas that of $C-C$ increases. Namely, as the carbonized temperature increases, the content of oxo-organic functional groups in the BPC substrate decreases and that of $C-C$ groups in the substrate increases. The -

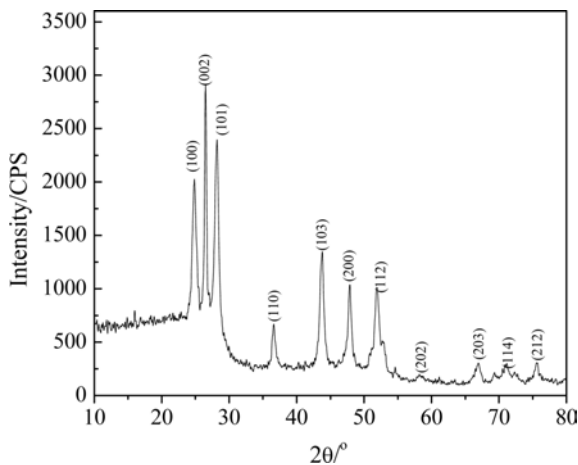


Fig. 2. XRD pattern of nano-CdS/BPC material.

CO₂ and C-O groups can serve as “active points” during the growth process of nano-materials [22].

XRD analysis of nano-CdS/BPC material

Fig. 2 shows the XRD pattern of the nano-CdS/BPC material (BPC substrate derived from pine, carbonized at 450 °C, 24 h growth time). The narrow and sharp peaks indicate a good crystalline state, which is consistent with the PCPDF standard card (No. 80.0006). The crystal parameters are $a = 4.14 \text{ \AA}$, $c = 6.67 \text{ \AA}$. All peaks are consistent with the small crystal size of CdS; additionally, peak (002) is stronger than the others, thus indicating that growth of the CdS crystal preferentially occurs along the c axis in the [001] direction to form a nanorod-CdS [26]. The grain size is calculated to be approximately 7 nm according to the Scherer formula. The low and weak diffraction peaks of the BPC substrate are covered by the CdS diffraction peaks [27].

Thermal decomposition behavior of nano-CdS clusters

Fig. 3 shows the TG-DTG and DSC curves for nano-CdS clusters obtained in solution. As shown in Fig. 3-a, there are three weight loss steps of the nano-CdS clusters in an inert atmosphere. The clusters exhibit an

initial weight loss below 79.40 °C due to the evaporation of residual water, organic solvent and absorbed gas. The TG curve exhibits a sharp decline between 663.10 and 758.70 °C for the decomposition of CdS to Cd. A slight increase in weight can then be observed at temperatures above 778.15 °C, which results from the reaction of Cd with a small amount of O₂ in the Ar atmosphere. Additionally, all weight loss for the decomposition and oxidization of CdS is in accordance with theoretical calculations.

The DSC curve of the material is shown in Fig. 3-b; the exothermic peaks appear at 443.50 and 766.70 °C, respectively. Combining the DSC curve with the TG-DTG curve, the peak at 443.50 °C corresponds to the phase transformation of CdS, the peak at 766.70 °C corresponds to the decomposition of CdS. Above 766.70 °C, there is an exothermic trend, which corresponds to the oxidation of Cd [28].

Influence of growth time on the microstructure of nano-CdS clusters

The microstructure of nano-CdS clusters obtained in solution with different growth times are shown in Fig. 4. As shown in Fig. 4-a, multi-arm-shaped nano-CdS clusters are obtained, the particle size is approximately 50 nm, and there is also slight agglomeration. After 24 h of growth, rod-shaped nano-CdS clusters can be obtained, having a width of approximately 20 nm and a length of approximately 200 nm, and there is extensive agglomeration (Fig. 4-b). After 48 h of growth, flower-shaped nano-CdS clusters are obtained, having a flower leaf thickness of approximately 100-120 nm and length ranging between 0.2 and 2 mm.

Namely, the size and shape of nano-CdS clusters can be controlled by the growth time. In the next step, the growth time for all processes of the nano-CdS clusters on BPC substrates is fixed at 24 h.

Influence of substrate type on the microstructure of nano-CdS/BPC material

Fig. 5 shows the microstructure of nano-CdS/BPC materials (BPC substrates derived from pine, bamboo

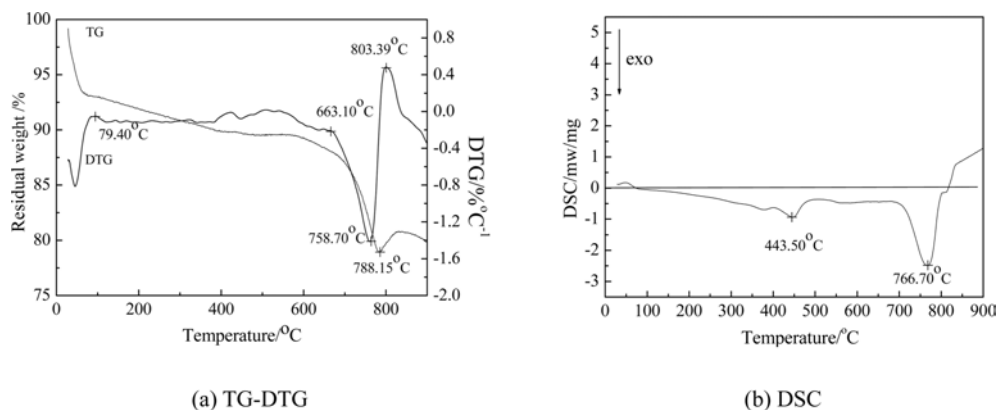


Fig. 3. TG-DTG and DSC curves of nano-CdS clusters obtained in solution.

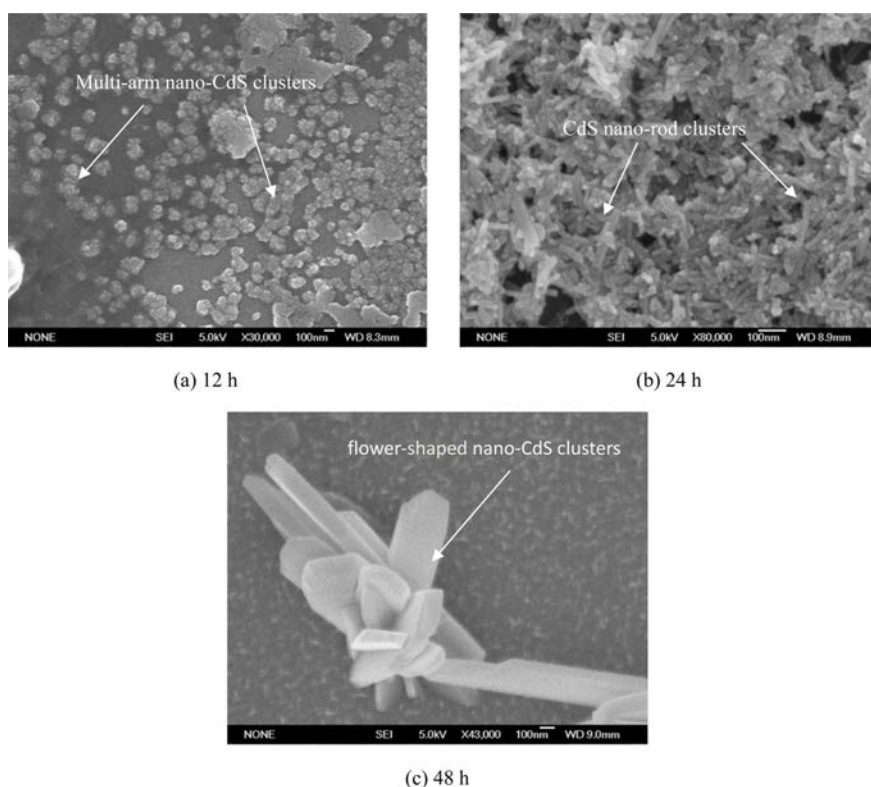


Fig. 4. SEM micrographs of nano-CdS clusters with different growth times.

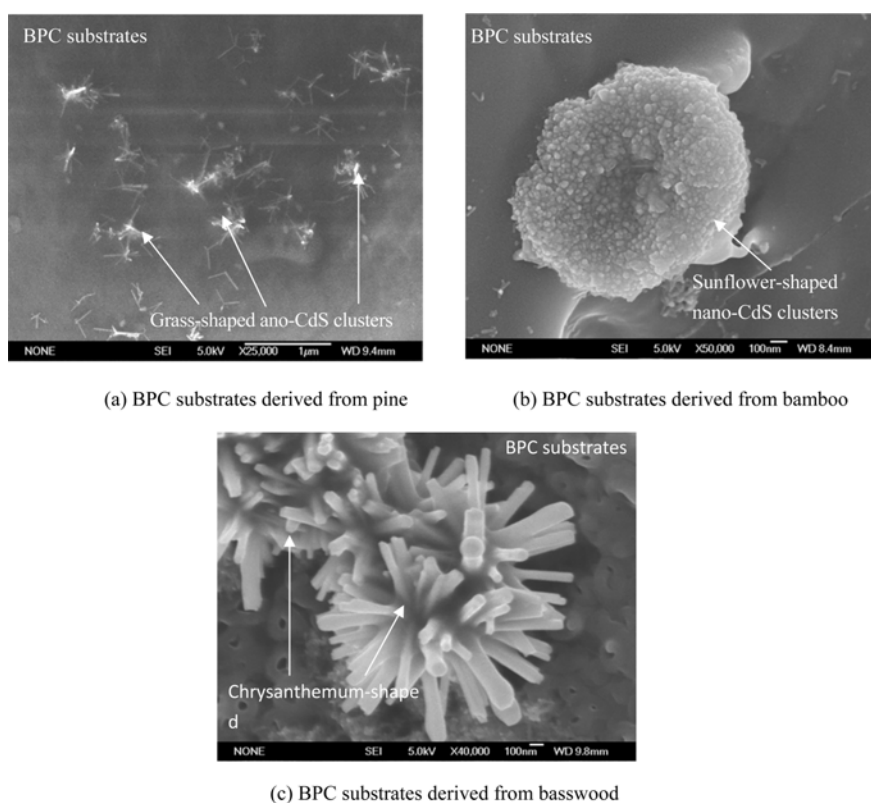


Fig. 5. SEM micrographs of nano-CdS clusters grown on BPC substrates derived from different types of wood.

and basswood, respectively, all carbonized at 450 °C).

Fig. 5-a depicts couch grass-shaped nano-CdS clusters that grow on the inner walls of BPC derived

from pine. The “grass” combines well with the surfaces of the walls and is uniformly distributed. The leaf length is approximately 200 nm, and the diameter is

Table 1. EDS data of nano-CdS clusters grown on BPC substrates (point EDS).

Sample	Element (Ratio of atom)		
	Cd	S	C
CdS on BPC substrates from pine	40	42	16
CdS on BPC substrates from bamboo	48	48	4
CdS on BPC substrates from basswood	47	47	6

approximately 10 nm. All clusters are very well dispersed without agglomeration. Perhaps the existing “active point” on the surface of the inner walls of BPC can serve as a “growth point” to avoid agglomeration.

In Fig. 5-b, sunflower-shaped nano-CdS clusters can be observed growing on the inner wall of BPC derived from bamboo. The particle size of the “seed” is approximately 10 nm, and that of the flower is approximately 1 μm. Additionally, we can see that the growth point is a small pore on the inner wall of the BPC substrate.

From Fig. 5-c, chrysanthemum-shaped nano-CdS clusters can be observed growing on the inner wall of the BPC substrate derived from basswood. The leaf diameter is approximately 60-100 nm and the length is approximately 0.5-1 μm. The clusters also adhere tightly to the surfaces of the walls of the BPC substrate.

Different morphologies of nano-CdS clusters can grow on different BPC substrates. This phenomenon may result from the microstructure, specific area, pore size, and organic group on the wall of BPC derived

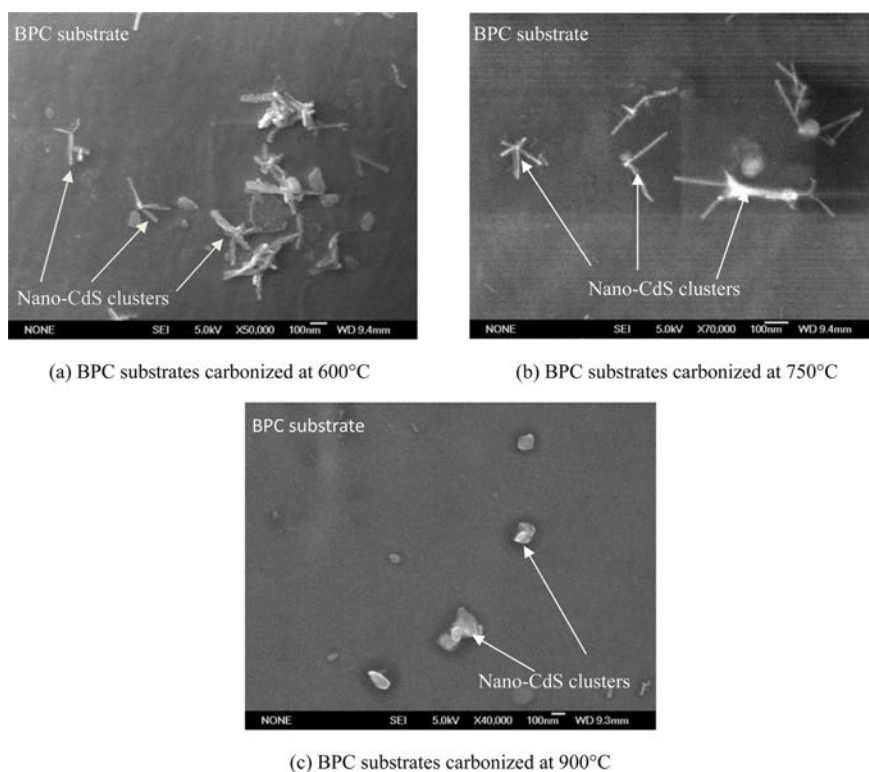
from different types of wood [24, 25, 29].

Tab. 1 lists the EDS data of nano-CdS clusters grown on BPC substrates (point EDS) (point EDS). From the data, it is clear that the main composition of the nano-materials is CdS and that the elemental carbon is from the BPC substrate.

Influence of the substrate carbonized temperature on the microstructure of nano-CdS/BPC materials

The microstructures of nano-CdS/BPC materials are shown in Fig. 6 (BPC derived from pine, carbonized at 600 °C, 750 °C and 900 °C, respectively). Combined with Fig. 5-a, the number of nano-CdS clusters on the inner walls of the BPC substrate decreases with increasing BPC carbonized temperature. There are abundant oxo-organic functional groups (such as O-C=O, C-O and C-O-C) in the BPC substrate when carbonized at 450 °C. A single pair of electrons on the O atom can coordinate with the Cd²⁺ cation as an “active point” to increase the nucleation rate of the CdS crystal [30].

With increasing carbonization temperature, the content of oxo-organic functional groups in BPC decreases. Namely, the number of “active points” decreases, which results in a decreased amount of nano-CdS clusters that grow on BPC substrates. When the carbonized temperature of BPC reaches 900 °C, most of the organic functional groups in BPC substrate decompose; as a result, it is difficult to grow CdS clusters on the inner wall of BPC substrates (Fig. 6-c).

**Fig. 6.** SEM micrographs of nano-CdS clusters grown on BPC substrates from pine carbonized at different temperatures.

Growth mechanism of nano-CdS clusters on the inner wall of BPC substrate

According to the model of the growth unit, the growth process of a crystal is that a coordination ion in solution deposits on the interface of nuclei as a growth unit; its coordination number is the same as that of an ion or atom in the crystal. *Cd* and *S* are present as $[CdS_4]$ and $[SCd_4]$, with tetrahedral coordination with *Cd* and *S* atoms existing in the center of the structure in the CdS crystal [30].

In this experiment, $En(H_2NCH_2CH_2NH_2)$, which acts as the coordinate reagent because of its high concentration and strong coordination ability, can react with Cd^{2+} through a single pair of electrons on the *N* atom that fills the 5*s* and 5*p* electronic orbitals of Cd^{2+} when the 5*s* and 5*p* orbits occur as sp^3 orbital hybrids. As a result, the stability of the electronic orbital for Cd^{2+} (fully occupied $4d^{10}$) decreases, and then S^{2-} can combine with Cd^{2+} and replace N to produce CdS [30].

First, Cd^{2+} and the *En* group in solution form ion complexes such as $[Cd(NH_2)_4]^{2+}$, then S^{2-} can replace NH_2 in ion complexes to connect with Cd^{2+} , the replacement reaction can occur slowly as all *En* groups in ion complexes are replaced. A schematic model of this process is shown below [31]:

From the above discussion, we know that the dangling bonds on each surface of the crystal are NH_2 . Thus, the growth rate of each face depends on the number of NH_2 groups depositing to the solution. According to the law of the growth rule and the coordination polyhedron, each face of the CdS crystal has a different number of angles, edges or faces exposed to the solution, so the growth rate in each direction is different. According to Ref [32], the growth rate in the *c*-axial [001] direction is the highest. As the growth time increases, the grains of CdS grow to become slender nano-rods, in accordance with the results in Ref [26].

When the BPC substrate is in the solution, it can work as an “active point” for a large specific area and abundant oxo-organic functional groups. A single electron pair on the *O* atom in an oxo-organic functional group can combine with a Cd^{2+} cation to increase the nucleation rate of the CdS crystal as seen in Fig. 5-a and Fig. 6-a and b. Additionally, the site of the “active point” is stable in BPC, which helps to prevent agglomeration of nano-crystal as seen in Fig. 4-b and Fig. 5-b. With increasing carbonized temperature, the content of oxo-organic functional groups on the BPC substrate decreases and results in a decrease in the amount and size of nano-CdS clusters growing on the inner walls of BPC.

The crystal nucleation and growth processes of the nano-CdS on BPC substrate are as follows:

Conclusions

1. As the carbonized temperature increases, the content of oxo-organic functional groups in the BPC substrate decreases, and that of C-C groups increases;
2. Couch grass-shaped nano-CdS clusters can grow on the inner walls of BPC substrates derived from pine; sunflower-shaped nano-CdS clusters can grow on those derived from bamboo; and chrysanthemum-shaped nano-CdS clusters can grow on those derived from basswood. The size and amount of nano-clusters on BPC substrates can be controlled by the growth time and carbonized temperatures of the substrate;
3. The growth mechanism of nano-CdS clusters on BPC substrates is that the *O* atom in the oxo-organic functional groups on the inner wall of BPC functions as an “active point” to bond with Cd^{2+} to increase the nucleation rate of CdS; *En* can subsequently coordinate with Cd^{2+} to decrease the electronic orbital stability of Cd^{2+} , and finally, S^{2-} can replace the *En* group to obtain the CdS crystal. There are different amounts of *En* groups based on the direction of the crystal faces, which leads to a different morphology of nano-CdS clusters. The stable “active point” in BPC can also help prevent agglomeration of nano-crystals.

Acknowledgments

This work is supported by the Natural Science Foundation of Hunan Province, China (Grant No. 12JJ4054), the Science and Technology Planning Project of Hunan Province, China (2012 WK3023) and the Planning of the Growth of Young Teachers (Hunan University China).

The authors also acknowledge Dr. Ming-jian Wu and Dr Xia Hua for useful discussions regarding the XPS results and for their assistance in revising this manuscript.

References

1. Wentao Zhang, Hong-Ro Lee. *J. Photochem. Photobiol., A: Chemistry*, 218 (1) (2011) 1-5.
2. Frédéric Dumur, Denis Bertin, Cédric R. Mayer, Audrey Guerlin, Guillaume Wantz, Gihane Nasr, Eddy Dumas, Fabien Miomandre, Gilles Clavier, Didier Gigmes. *Synth. Met.* 16 (17-18) (2011) 1934-1939.
3. Min Zhong, Dong Yang, Jian Zhang, Jingying Shi, Xiuli Wang, Can Li. *Sol. Energy Mater. Sol. Cells.* 96 (2012) 160-165.
4. A.S. Obaid, Z. Hassan, M.A. Mahdi, M. Bououdina. *SOL ENERGY* 89 (2013) 143-151.
5. Sudipto Das, Suvendu Samanta, Swarup Kumar Maji, Partha Kumar Samanta, Amit Kumar Dutta, Divesh N. Srivastava, Bibhutoh Adhikary, Papu Biswas. *Tetrahedron Lett.* 54 (9) (2013) 1090-1096.
6. Lei ZHU, Ze-da MENG, Kwang-youn CHO, Won-chun OH. *NEW CARBON MATER.* 27 (3) (2012) 166-174.
7. M. Lei, P.G. Li, W.H. Tang, *J. Alloys Compd.* 509 (15)

- (2011) 5020-5022.
8. N. Srinivasan, S. Thirumaran, Samuele Ciattini. *J. Mol. Struct.* 1026 (2012) 102-107.
 9. Akram Hosseinian, Ali Reza Mahjoub. *J. Mol. Struct.* 985 (2-3) (2011) 270-276.
 10. Q. C. Kong, R. Wu, X.M. Feng, C. Ye, G.Q. Hu, J.Q. Hu, Z.W. Chen, *J. Alloys Compd.* 509 (6) (2011) 3048- 3051.
 11. Anukorn Phuruangrat, Nuengruethai Ekthammathat, Titipun Thongtem, Somchai Thongtem. *J. Alloys Compd.* 509 (41) (2011) 10150-10154.
 12. Fengzhen Liu, Xin Shao, Jinqing Wang, Shengrong Yang, Huaiyong Li, Xianhua Meng, Xuehua Liu, Min Wang. *J. Alloys Compd.* 551 (2013) 327-332.
 13. Weinan Xing, Liang Ni, Pengwei Huo, Ziyang Lu, Xinlin Liu, Yingying Luo, Yongsheng Yan. *Appl. Surf. Sci.* 259 (2012) 698-704.
 14. R. Marx Nirmal, K. Pandian, K. Sivakumar. *Appl. Surf. Sci.* 257 (7) (2011) 2745-2751.
 15. Ahed Zyoud, Iyad Saa'deddin, Sahar Khudruj, Zafer M. Hawash, DaeHoon Park, Guy Campet, Hikmat S. Hilal. *SOLID STATE SCI.* 18 (2013) 83-90.
 16. Xiaohui Wang, Dong Li, Yanzhu Guo, Xiaoying Wang, Yumin Du, Runcang Sun. *Opt. Mater.* 34 (4) (2012) 646-651.
 17. R. Castro-Rodríguez, J. Mendez-Gamboa, I. Perez-Quintana, R. Medina-Ezquivel. *Appl. Surf. Sci.* 257 (22) (2011) 9480-9484.
 18. Y.A. El-Gendy, I.S. Yahia, F. Yakuphanoglu. *Mater. Res. Bull.* 47 (11) (2012) 3397-3402.
 19. S.H. Mohamed, E.R. Shaaban. *Physica B: Condensed Matter*, 406 (22) (2011) 4327-4331.
 20. W. X. Zhao, Z.P. Bai, A.L. Ren, B. Guo, C. Wu, *Appl. Surf. Sci.* 256 (11) (2010) 3493-3498.
 21. B. C. Huang, Y. Yang, X. S.Chen, D.Q.Ye, *Catal. Commun.* 11 (9) (2010) 844-847.
 22. M. Li, Y.L. Liu., P. Z. Gao, W. Chen, Z. X Fu . *Rare Met. Mater. Eng.* 38 (4) (2009) 734-737.
 23. P. Z. Gao, Y. M. Bai, S. Lin. *Ceram. Int.* 34 (2008) 1975-1981.
 24. P. Z. Gao, M. J. Wu, B. J. Li, Y.L. Liu. *Mater.Res. Bull.* 44 (2009) 644-648
 25. Wagner C D, Riggs W M, Davis L E, et al. *Muilenberg, Handbook of X-Ray Photoelectron Spectroscopy*[M]. Prairie: Perkin-Elmer, 1978
 26. M.A. Mahdi, J.J. Hassan, Naser M. Ahmed, S.S. Ng, Z. Hassan. *Superlattices Microstruct.* 54 (2013) 137-145.
 27. Z.J. Li, Z.F. Hu, F. J. Liu, J. Sun, H. Q. Huang, X. Q. Zhang, Y. S.Wang, *Mater. Lett.* 65 (2011) 809-811.
 28. G. S. Paul, P. Gogoi , P. Agarwal, *J. Non-Cryst. Solids* 354 (2008) 2195-2199.
 29. A.W.M. Ip, J.P. Barford, G. McKay, *Bioresource Tech.* 99 (18) (2008) 8909-8916.
 30. Q.L. Nie, Q.L. Yuan, W.X. Chen, Z.D. Xu,J. *Cryst. Growth* 265 (2004) 420-424.
 31. Q.Q.Wang, G. Xu, G.R.Han, *J. Solid State Chem*,178 (2005) 2680-2685.
 32. H. Zhang, X.Y. Ma, Y.J. Ji, J. Xu, D.R Yang, *Chem. Phys. Lett.*377 (2003) 654-657.